

Yielding and irreversible deformation below the microscale: Surface effects and non mean-field plastic avalanches

Paolo Moretti^{1,2}, Benedetta Cerruti^{1,3}, M. Carmen Miguel¹

¹Departament de Física Fonamental, Facultat de Física, Universitat de Barcelona
Diagonal 647, E-08028, Barcelona, Spain

²Departament de Física i Enginyeria Nuclear, Universitat Politècnica de Catalunya
Campus Nord B4, E-08034, Barcelona, Spain

³Institute for Cancer Research and Treatment
Strada Provinciale 142, 10060 Candiolo (TO), Italy

Abstract.

Nanoindentation techniques recently developed to measure the mechanical response of crystals under external loading conditions reveal new phenomena upon decreasing sample size below the microscale. At small length scales, material resistance to irreversible deformation depends on sample morphology. Here we study the mechanisms of yield and plastic flow in inherently *small* crystals under uniaxial compression. Discrete structural rearrangements emerge as series of abrupt discontinuities in stress-strain curves. We obtain the theoretical dependence of the yield stress on system size and geometry and elucidate the statistical properties of plastic deformation at such scales. Our results show that the absence of dislocation storage leads to crucial effects on the statistics of plastic events, ultimately affecting the *universal* scaling behavior observed at larger scales.

1. Introduction

Over the past years, experimental investigations have gathered increasing evidence that plastic deformation of crystalline materials proceeds through intermittent bursts of activity [1, 2, 3, 4, 5, 6, 7, 8]. Plastic flow advances through a sequence of strain avalanches of broadly distributed sizes. Avalanches have been observed experimentally under stress control conditions at various scales. Although such plastic fluctuations may be hard to detect at macroscopic scales, they dramatically affect mechanical properties of crystalline materials at smaller scales, ultimately producing detrimental effects on material formability [9]. The introduction of microcrystal compression testing [4] has allowed access to the microscale and introduced sample size as a crucial variable in this scenario. Size effects have dramatic consequences on yield, making smaller samples harder to deform and more unpredictable [6]. It is then natural to wonder if such behavior would hold unchanged below the micrometer scale.

While several nanoindentation techniques have been developed to measure material resistance to irreversible deformation and plastic flow, the experimental observation of plasticity at the nanoscale still represents an enormous challenge [10]. Colloidal crystals, however, were proven to deform plastically by activating dislocation motion, in remarkable analogy with crystalline materials [11, 12, 13, 14]. The unmatched advantage of working with such systems is brought in by their size. Micrometer-sized colloidal crystals may contain few thousands, or even hundreds, of particles. This aspect allows one to project the problem of nanomechanics into a length scale that is easily accessible on experimental grounds. In this work, we address some of the challenges posed by nanomechanics, by providing a theoretical study of the mechanisms of yield and plastic flow in inherently *small* systems. We propose a simple geometry, which can be reproduced in experiments on two-dimensional micrometer colloidal crystals, and provide robust input for mechanical testing of crystalline thin films below the micrometer scale. Our aim is to show that at very small scales the irreversible deformation of materials proceeds in a novel way, deviating from the allegedly universal behavior observed in larger systems. To this end, we investigate the dependence of the yield stress on system size and geometry and the statistical properties of plastic deformation and energy dissipation in uniaxially compressed two-dimensional *small* crystals, by means of atomistic simulations and analytical modeling.

2. Elastic loading and plastic yield

2.1. Simulation method

We first consider the compression of perfect crystals of various sizes and aspect ratios. Crystals are simulated as two-dimensional aggregates of short-range interacting monodisperse particles in their lowest energy configuration, that is a triangular lattice in the xy plane. Boundaries parallel to the y direction are in contact with rigid walls, while those parallel to the x direction are free (see Fig. 1). Uniaxial compression is

applied symmetrically along the x direction. We consider two different compression protocols: i) displacement-control, in which rigid walls are quasi-statically displaced at equal constant velocities in opposite directions; ii) force-control, in which the force exerted on the walls is slowly increased at a constant driving rate. We consider a set of

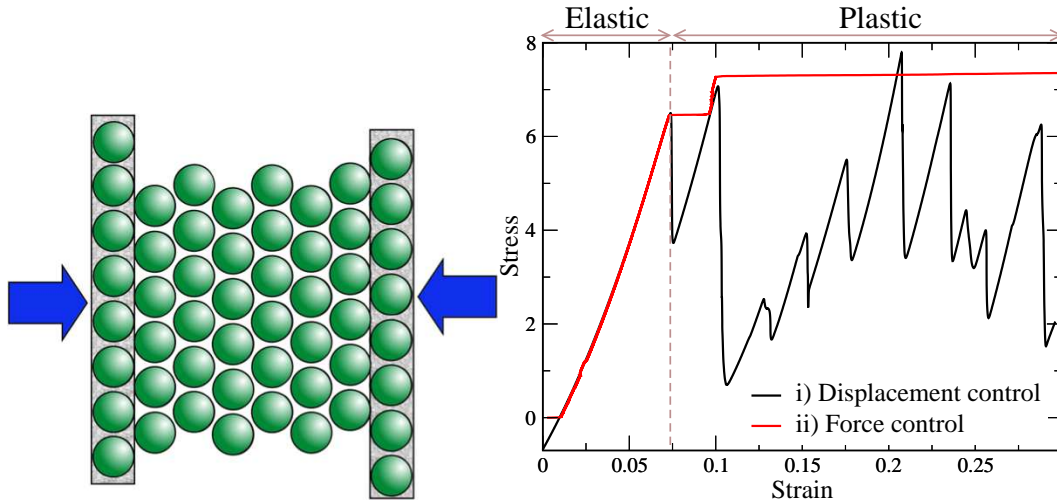


Figure 1. Stress strain curves. (Left) Schematic representation of a uniaxial compression test on a perfect crystal monolayer. (Right) We obtain i) a serrated-flow stress response under displacement (or strain) control conditions, i.e. ruling the position of the bounding walls (inside the grey boxes), or ii) a staircase shaped curve under force or stress control conditions, i.e. regulating the applied force on the driving walls. The dashed line signals the location of the yield point.

N particles located at the nodes of a triangular lattice and confined between two rigid walls (as in Fig. 1). Particles interact pairwise through a short-range potential V_{ij} . For simplicity, we use a Lennard-Jones potential, but any other short-range one would lead to qualitatively similar results. We implement overdamped dynamics simulations. This choice is inspired by experiments on colloids, in the presence of a viscous carrier fluid. However, since we drive our system quasi-statically, we expect molecular dynamics simulations in the canonical ensemble (as for crystalline metals and alloys) to produce analogous results. The equation of motion for each particle i at position \mathbf{r}_i

$$\Gamma \frac{d\mathbf{r}_i}{dt} = \sum_j \mathbf{f}\left(\frac{\mathbf{r}_i - \mathbf{r}_j}{d}\right) + \mathbf{f}_d(\mathbf{r}_i), \quad (1)$$

where Γ is the viscous friction coefficient of the carrier fluid, f is the interparticle force, d the characteristic size of the particles, and f_d is the corresponding driving force for each deformation protocol. We choose as units of space and time d and $t_0 = \Gamma d^2/V_0$ respectively, with V_0 the amplitude of the inter-particle potential, and we measure the driving force f_d in units of V_0/d . In dimensionless units, the linear system sizes L_x^0 considered range from $L_x^0 = 16$ to $L_x^0 = 72$. Particles are confined by two rigid walls, that we model as two extra columns of particles of the same size, commensurate with the crystalline planes (see Fig. 1). In displacement control simulations, rigid walls are

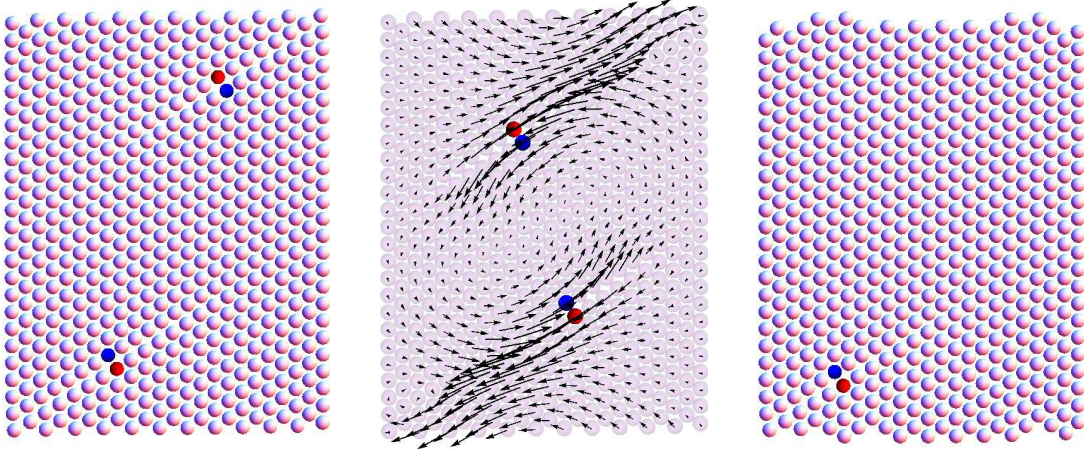


Figure 2. Dislocation nucleation at yield. (Left) Perfect crystal, a dislocation pair is nucleated. Dislocations are represented as pairs of 5- and 7-coordinated particles, in blue and red respectively. (Center) Instantaneous velocity field of the particles. (Right) Surface-disordered crystal, dislocations may be individually nucleated at surface steps.

driven quasi-statically with a constant velocity $v = 0.005$ in simulation units, whereas in the force control simulations the force exerted on the walls is slowly increased at a constant driving rate equal to 0.005. In both cases, these values are sufficiently small to avoid the overlap of plastic events. Smaller driving rates do not yield significantly different results.

The coupled Eqs. (1) for $i = 1, \dots, N$ are integrated numerically with an adaptive step size fifth-order Runge-Kutta method with precision 10^{-6} . Thermal and hydrodynamic effects on the particles have been neglected. Thermal fluctuations can be disregarded because the characteristic time for dislocation motion is much faster than the characteristic time for thermal diffusion. Moreover in the problem at hand, elastic interactions would prevail over hydrodynamic interactions between the particles, if in suspension.

2.2. Yield stress and sample geometry

In both protocols, the response is initially elastic. In a perfect crystal, the elastic limit is reached as soon as the motion of a pair of opposite sign edge dislocations is activated, as in Fig. 2, marking the beginning of the irreversible or plastic flow regime [24]. We use this limit to define the yield stress σ_y and the yield strain γ_y of the crystal.

By moving, dislocations allow the system to slip plastically and emit/dissipate part of the stored elastic energy. The value of both the yield stress σ_y and strain γ_y are found to be independent of the deformation protocol. Figure 3 shows the dependence of the yield stress on the geometry of the sample under examination. Different systems sizes L and aspect ratios ρ are considered. Even below the microscale, we qualitatively recover the inverse size dependence of the yield stress that makes smaller samples stronger.

According to the literature, In larger systems the dependence of the yield stress on

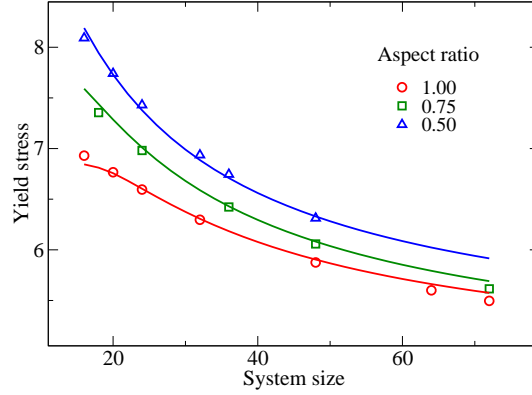


Figure 3. Yield stress in our nano-scale geometry. Smaller systems are stronger, but also different aspect ratios ρ induce different yield patterns. Discrete data: simulation results. Solid lines: theoretical predictions (see main text).

the system size follows a power law [6], which corroborates the view of plastic yield as a critical phenomenon, dominated by scale free rearrangements of dislocation patterns over finite-size effects [15]. Plasticity is dominated by bulk phenomena and surfaces are somehow peripheral to such mechanisms. At smaller scales, our results show instead that σ_y is strongly affected by both size and geometry of the specimen. Size effects at this length scale were experimentally observed in compression tests in gold nanopillars [16], which were able to relate the increase in hardness to the *dislocation starvation* mechanism. Figure 2 shows that in our systems yield is mediated by a single dislocation pair (or even by a dislocation alone in the case of an imperfect crystal) and the onset of plasticity does not require the collective motion of a complex dislocation network. Dislocation interplay with boundaries thus becomes crucial. Early studies showed that the interaction of dislocations with rigid substrates is inherent to the strengthening of sheared thin films [17, 18]. Nevertheless, the role of rigid boundaries in uniaxial compression experiments is still a matter of investigation.

The connection between the yield stress and the boundary effects can be easily visualized in our simple model system. Up to values of the stress very close to σ_y , the behavior of the system is elastic and the strain energy is approximated by

$$E_e(\sigma_y) \approx \sigma_y^2 \frac{S}{2Y_\rho}, \quad (2)$$

where S is the specimen surface and Y_ρ is the effective Young modulus. At yield the onset of dislocation motion is almost instantaneous compared to the dynamics of steady loading. Dislocations must account for the stress distribution inside the compressed sample, giving rise to the elastic energy density \mathcal{E} . However, before dislocation motion is initiated, the elastic energy stored in the dislocated system must be comparable to the energy E_e right before yield, as approximately no dissipation has occurred yet. This leads to the simple relation

$$E_e(\sigma_y) \approx \int \int_s \mathcal{E} dx dy. \quad (3)$$

Equation (3) establishes a connection between the yield stress and dislocation strain distribution. It also bears implicitly the information about the dependence of the yield stress on the system size and geometry. The essence of the problem lies in the stress distribution that accounts for \mathcal{E} . In particular, an anomalous stress concentration is required at rigid boundaries, in order to enforce the condition of vanishing displacements. It is evident that boundary conditions alter dramatically the energy landscape \mathcal{E} in the specimen and ultimately affect the yield stress, as prescribed by Eq. (3).

2.3. An estimate of the yield stress

By means of elasticity theory, we can demonstrate that the stress fields produced inside the sample by an edge dislocation close to a rigid boundary are long ranged and decay as $\sim 1/r$, thus showing no screening effects, unlike dislocations close to free boundaries [19]. For simplicity, we consider a positive straight edge dislocation with Burgers vector perpendicular to the rigid wall, a distance l apart from the wall, as in Fig. 4 (left). The problem has translational invariance along the z direction (plane strain conditions): the wall is at $x = 0$, the dislocation is placed in $(l, 0, z)$. We can calculate the exact displacement field \mathbf{u} as $\mathbf{u} = \mathbf{u}^{inf} + \mathbf{u}^{img} + \mathbf{w}$ where \mathbf{u}^{inf} is the displacement field of the original positive dislocation in $(l, 0, z)$ in an infinite medium, \mathbf{u}^{img} is the displacement of the image dislocation of opposite sign in $(-l, 0, z)$ and \mathbf{w} is an additional field, which is analytic in $x > 0$ and satisfies the equilibrium elastic equations

$$\mu \nabla^2 \mathbf{w} + (\lambda + \mu) \nabla (\nabla \cdot \mathbf{w}) = 0, \quad (4)$$

with boundary conditions such that the full $\mathbf{u}(0, y, z) = 0$, being μ the shear modulus and ν the Poisson ratio. Eq. (4) with the given boundary conditions is commonly known as the 1-plane problem in linear elasticity. Several techniques can be devised to find exact solutions [20] and the complexity resides solely on the complicated form of boundary conditions. Here we follow [21] as reviewed by [20] and observe that Eq. (4) can be rewritten as a Laplace equation in the form

$$\nabla^2 \left[\mathbf{w} + \frac{\lambda + \mu}{2\mu} \begin{pmatrix} x \\ y \\ z \end{pmatrix} \vartheta \right] = 0, \quad (5)$$

where $\vartheta = \nabla \cdot \mathbf{w}$ is the dilatation. The problem can then be solved using the Green function method, being the Green function for Eq. (5) in the 1-plane geometry known from classical electrostatics. While further details will be given in a future publication [22], for the problem at hand we obtain

$$\begin{aligned} w_x &= \frac{1}{\pi} \left[\arctan \frac{y}{l+x} + \frac{1}{2(1-\nu)} \frac{ly}{(l+x)^2 + y^2} \right] + \\ &\quad + \frac{x}{\pi(3-4\nu)} \left[\frac{y}{(l+x)^2 + y^2} + \frac{l}{2(1-\nu)} \frac{2y(l+x)}{[(l+x)^2 + y^2]^2} \right] \\ w_y &= -\frac{x}{\pi(3-4\nu)} \left[\frac{l+x}{(l+x)^2 + y^2} + \frac{l}{2(1-\nu)} \frac{(l+x)^2 - y^2}{[(l+x)^2 + y^2]^2} \right] \end{aligned} \quad (6)$$

$$w_z = 0.$$

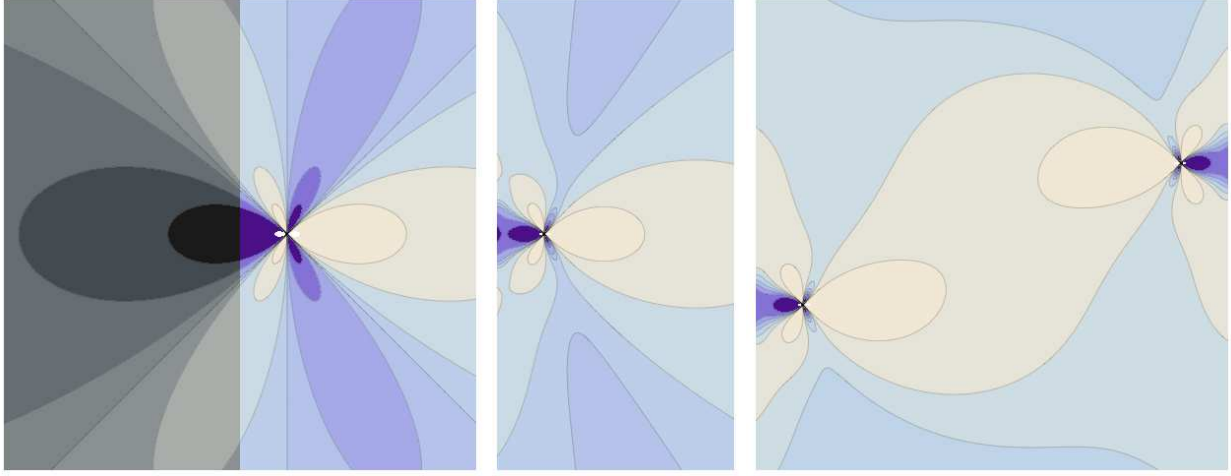


Figure 4. (Left) Shear stress distribution around an edge dislocation in an infinite medium. The right side of the picture is shaded, indicating that we are interested in how the stress field changes upon imposing a rigid boundary. (Center) Shear stress distribution around an edge dislocation located near a rigid boundary. (Right) Shear stress distribution due to a pair of opposite sign dislocations, confined within two rigid walls. Stresses rapidly vanish in the y direction. Color code: Lighter regions indicate positive stresses, darker regions negative stresses. Vanishing stresses are represented in light blue. Curves of equal stress are represented as a guide to the eye. For simplicity, the case of Burgers vectors perpendicular to the walls was considered here.

From the above result, the strain and stress tensor components ε_{ij} and σ_{ij} and the elastic strain energy density can be calculated using linear elasticity. Interestingly, while the stress components derived from $\mathbf{u}^{inf} + \mathbf{u}^{img}$ decay like $\sim 1/r^2$ (being that the stress of a dislocation dipole), the stress due to \mathbf{w} will decrease like $\sim 1/r$. Overall, the stress field of an edge dislocation close to a rigid boundary will hence be long-ranged, as opposed to the case a free boundary. As a consequence, stress fields are able to sample the entire system size and are responsible for the size-sensitivity of the yield stress.

In the case of our simulations, however, Eq. (6) may seem of little help in calculating the strain energy \mathcal{E} at yield for our model system, where we have two fixed boundaries, two free surfaces and two dislocations of opposite signs, as the exact solution of such a problem would be great complexity. Nevertheless, an approximation of the integral in Eq. (3) can be provided as follows. Fig. 4 (right) shows the result of the superposition of the solutions for the shear stress of two edge dislocations of opposite signs, as calculated from Eq. (6), arranged in a configuration which mimics the one observed at yield in our simulations for the perfect crystal. For simplicity we consider Burgers vectors along x , but the general solution would lead to similar results [22]. In such a configuration, the condition of zero displacement at the vertical walls is not met anymore, however one can prove that the deviations from zero affect the stress and the strain energy in a negligible way if the dislocations are far apart. At the same time, Fig. 4 (right)

shows that the two dislocations behave like a dipole, in the sense that the stress goes rapidly to zero outside the region enclosed by them, approximating the stress field close to free boundaries. Such observation is verified analytically and is valid for all stress components.

We can conclude that the configuration in Fig. 4 (right) provides an acceptable approximation for the elastic problem in our simulations and an estimate for the strain energy \mathcal{E} in Eq. (3). Finally, upon inverting Eq. (3) and computing numerically the integrals of \mathcal{E} , we evaluate the yield stress and its dependence on the system size and geometry. Results are given in Fig. 3 and are in remarkably good agreement with the previously discussed simulation results, suggesting that boundaries and shape effects are essential in our problem. Given the nature of the approximations involved, we stress that ours is just a dimensional estimate. However the agreement with simulations corroborates the view that the role played by boundaries is integral to nanoplasticity.

3. Plastic avalanches

As soon as the yield point is reached, the response of the system to further loading differentiates depending on the deformation protocol. Under conditions of displacement control, stress-strain curves are characterized by serrated yielding, while they assume a staircase shape under conditions of stress control. We emulate realistic realizations of compressed samples by introducing randomness at free boundaries, keeping the number of particles constant. Strain plateaus $\Delta\gamma$ in force control or stress drops $\Delta\sigma$ in displacement control always correspond to plastic events in which dislocation motion is reactivated in order to reduce the elastic energy stored during prior loading phases (see Fig. 1). Remarkably, a statistical analysis of event sizes over several realizations of surface disorder (Fig. 5) reveals that sizes are power-law distributed as

$$p(\Delta\sigma) \sim \Delta\sigma^{-\tau_\sigma} \quad p(\Delta\gamma) \sim \Delta\gamma^{-\tau_\gamma}. \quad (7)$$

Due to the limited system size, moving dislocations easily leave the sample through free boundaries. Pioneering studies have shown that in sub-micrometer Ni samples, pure mechanical loading can induce dislocation depletion within the sample [23]. In our case plastic flow proceeds through the activation and motion of few dislocations at a time, while no storage is observed [24]. Such phenomenology differs from the widely accepted picture of plastic flow at larger scales. Yet, our statistical study leads to broadly distributed plastic events for several system sizes, suggesting that kinematic constraints and long range dislocation interactions still rule plastic flow, as shown in Fig. 5. The cumulative distribution is defined as $p_c(x) = \int_0^x p(x')dx'$. Upon a closer inspection, a noticeable difference in the exponent value is nevertheless encountered.

Plastic event sizes are commonly quantified in experiments by looking at the amount of energy W_{dis} released during each event or, under stress control conditions, by recording the magnitude of platen displacements. By definition, platen displacements under quasi-static loading identify plastic strain $\Delta\gamma_p$, while it can be shown that approximately

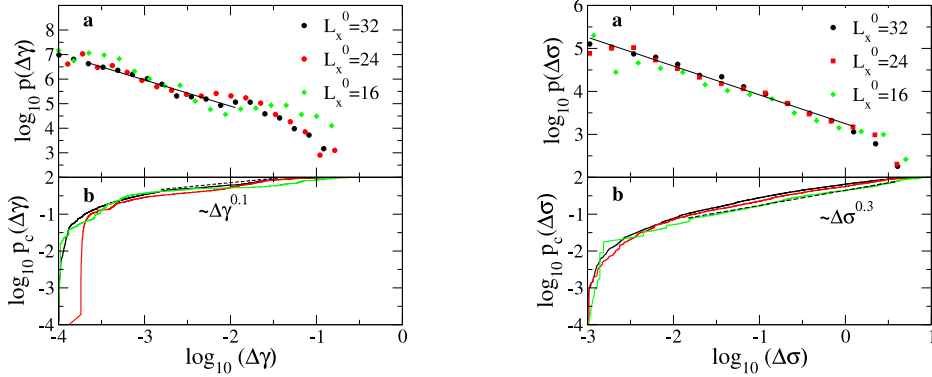


Figure 5. Statistics of plastic events. Left: (a) Distribution of platen displacements $p(\Delta\gamma)$ in force-control simulations, decaying with an exponent $\tau_\gamma \approx 0.9$. (b) Cumulative distribution p_c of platen displacements. Right: (a) Distribution of stress drops in displacement-control simulations, decaying with an exponent $\tau_\sigma \approx 0.7$. (b) Cumulative distribution of stress drops $p_c(\Delta\sigma)$.

$W_{dis} \sim \Delta\gamma_p$, as the amount of slip due to a moving dislocation is proportional to the energy dissipated in the process [25]. This relation indeed holds in our model, as shown in Fig. 6(a). Experimental studies at larger scales show that both quantities follow a power-law distribution, decaying with an exponent close to the mean-field value $\tau = 3/2$ [25]. The striking aspect of the exponent τ is its universality [9]. In our model, which aims to reproduce nanoscale plastic flow, the exponent $\tau_\gamma \sim 0.9$ deviates substantially from the universal value, suggesting that at such scales the microscopic dislocation dynamics giving rise to plastic deformation are qualitatively different. Signals of universality breakdown also come from experiments of compressed high-purity LiF micropillars [26]. Under displacement control conditions, the statistical analysis of plastic flow and dissipated energy can be performed by looking at the distribution of stress drops (Fig. 5(b)). In Fig. 6(b) we show the evolution of the energy balance during compression. For quasi-static driving, stress drops occur almost instantaneously, i.e. at constant total strain ($\Delta\gamma \simeq 0$, or $W_{ext} \simeq 0$). This implies that a sudden decrease of the elastic strain $\Delta\gamma_{el}$ of the crystal must occur at the expense of increasing its plastic strain, $\Delta\gamma_{el} \simeq \Delta\gamma_p$. Moreover, the energy dissipated by plastic avalanches must balance the change of internal energy, $dW_{dis} \simeq \Delta U$. Simple elasticity considerations allow one to conclude that $\Delta U \propto (\Delta\sigma)^2$ and obtain the following exponent relation $\tau_E = (\tau_\sigma + 1)/2$ for the dissipated energy distribution, which for $\tau_\sigma \sim 0.7$ yields $\tau_E \sim 0.85$, in good agreement with the results obtained for τ_γ in the force control protocol. In passing, we

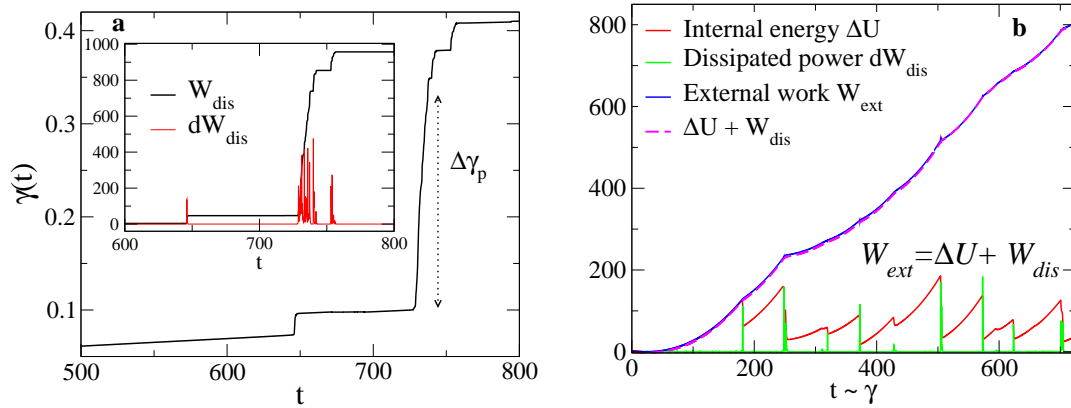


Figure 6. (a) Temporal evolution of the nominal strain γ and (inset) the dissipated energy in a force control compression test. In the quasi-stationary limit, platen displacements occur at constant stress and the dissipated energy is proportional to the increase of plastic strain. (b) Energy balance in a displacement control compression test. Stress drops occur at almost constant strain.

notice that an energy release exponent very close to 1 has been recently encountered in simulations of yielding and failure of heterogeneous materials in the plastic steady state [27]. However the rationale behind the analogy with our finding remains to be ascertained.

4. Conclusions

In conclusion, we have shown that the onset of plasticity at small scales is mediated by few dislocations. The number and arrangement of nucleated dislocations must account for the distribution of stress stored inside the crystal during the elastic-loading regime, allowing one to estimate the dependence of the yield stress on sample size and geometry. Our results confirm that both size and shape are crucial factors in determining the strength of materials at these scales. We find that plastic flow occurs in an intermittent manner reminiscent of irreversible deformation at larger length scales. Plastic avalanches of broadly distributed sizes are still observed, however, the absence of dislocation storage has important effects on the scaling characteristics of viscoplastic dynamics, which ultimately violate the *universal* mean-field behavior observed at larger scales. The new exponent values are obtained for a two-dimensional crystal geometry and should be relevant for thin films of several self-assembled nanoparticles under external loading conditions and amenable of experimental analysis in colloidal systems.

The Authors are grateful to M. Zaiser, L. Laurson and I. Groma for stimulating discussions. Financial support by the Ministerio de Educación y Ciencia (Spain), under Grant No. FIS2007- 66485-C02-02 and by a Spanish-Hungarian Integrated Action, under Grant No. HH2008-0002 is acknowledged. M.C.M. also acknowledges the Generalitat de Catalunya and the Ministerio de Educación y Ciencia (Programa I3) for additional funding.

References

- [1] Weiss J, Grasso J R, 1997 J. Phys. Chem. B **101** 6113
- [2] Miguel M C, Vespignani A, Zapperi S, Weiss J, Grasso J R, 2001 Nature **410** 667
- [3] Weiss J, Marsan D, 2003 Science **299** 89
- [4] Uchic M D, Dimiduk D M, Florando J N, Nix W D, 2004 Science **305** 986
- [5] Richeton T, Weiss J, Louchet F, 2005 Nat. Mater. **4** 465
- [6] Dimiduk D M, Woodward C, LeSar R, Uchic M D, 2006 Science **312** 1188
- [7] Richeton T, Dobron P, Chmelik F, Weiss J, Louchet F, 2006 Mater. Sci. Eng. A **424** 190
- [8] Schwerdtfeger *Jet al.* 2007 J. Stat. Mech. L04001
- [9] Csikor F F, Motz C, Weygand D, Zaiser M, Zapperi S, 2007 Science **318** 251
- [10] Cook R F, 2010 Science **328**, 183.
- [11] Schall P, Cohen I, Weitz D A, Spaepen F, 2004 Science **305** 1944
- [12] Pertsinidis A, Ling X S, 2005 New Journal of Physics **7** 33
- [13] Schall P, Cohen I, Weitz D A, Spaepen F, 2006 Nature **440** 319
- [14] Suresh S, 2006 Nat. Mater. **5** 253
- [15] Laurson L, Miguel M C, Alava M J, 2010 Phys. Rev. Lett. **105** 015501
- [16] Greer J, Nix W D, 2006 Phys. Rev. B **73** 245410
- [17] Nix W D, 1998 Scripta Materialia **39** 545
- [18] Nicola L, Van der Giessen E, Needleman A, 2003 J. Appl. Phys. **93** 5920
- [19] Hirth J P, Lothe J, 1982 *Theory of Dislocations*, Wiley & Sons
- [20] Love A E H, 1944 *A Treatise on Mathematical Theory of Elasticity*, Dover, New York
- [21] Tedone O, 1903 Ann. Mat. Pura Appl. (1898-1922) **8** 129-180
- [22] Moretti P, Miguel M C, In preparation.
- [23] Shan Z W, Mishra R, Syed Asif S A, Warren O L, Minor A M, 2008 Nature Mater. **7** 115
- [24] See supplementary movies.
- [25] Zaiser M, Moretti P, 2005 J. Stat. Mech. P08004.
- [26] Dimiduk D M, Nadgorny E M, Woodward C, Uchic M D, Shade P A, 2010 Philos. Mag. **90** 3621
- [27] Picallo C, López J M, Zapperi S, Alava M, 2010 Phys. Rev. Lett. **105** 155502